Two-temperature time-fractional model for electron-phonon coupled interfacial thermal transport

Milad Mozafarifard [a], Yiliang Liao [b], Qiong Nian [c], and Yan Wang [a, *]

[a] Department of Mechanical Engineering, University of Nevada, Reno, Reno, NV 89557, USA

[b] Department of Industrial & Manufacturing Systems Engineering, Iowa State University, Ames, IA 50011, USA

[c] School of Engineering for Matter, Transport and Energy, Arizona State University, Tempe, AZ 85287, USA

[*]**Corresponding author:** Yan Wang, Department of Mechanical Engineering, University of Nevada, Reno, Reno, NV 89557, USA

Email address: yanwang@unr.edu

Abstract

This research investigates electron-phonon coupled thermal transport in heterogeneous systems under femtosecond laser pulses. A two-temperature time-fractional (2T-TF) model based on the Caputo fractional derivative is presented, which is validated against experimental data and two-temperature Boltzmann transport equation (2T-BTE) results. The 2T-TF model is demonstrated to be more accurate than the diffusive two-temperature (2T) model based on Fourier's law, while its complexity can be much lower than 2T-BTE simulations. Moreover, various forms of thermal resistances can be readily implemented to the 2T-TF model. Using multi-layer metal-nonmetal thin films as model systems, we demonstrate that our 2T-TF model can reliably predict electron-phonon coupled thermal transport across metal-metal and metal-nonmetal interfaces as well as electron cooling in the top metallic layer after ultrafast laser irradiation. The 2T-TF model can serve as a convenient and reliable tool for simulating electron-phonon coupled thermal transport in heterogeneous systems that are vastly seen in laser manufacturing and micro-/nano-electronic devices.

1. Introduction

Micro- and nano-scale thermal transport has been an active research area and substantial efforts have been devoted to understanding properties and behaviors of heat carriers as well as the interactions between different heat carriers, particularly, electrons and phonons [1-4]. The study of electron-phonon interaction (EPI) is essential to ultrafast laser processing technologies because EPI directly determines the thermal transients during processing, which ultimately determines the microstructure [5-7]. Moreover, EPI is an important factor to consider for the thermal design of micro-/nano-scale electronic and photonic devices, as revealed by recent studies [8-11]. Notably, EPI is a crucial part of laser-material interaction, which is the foundation of laser manufacturing and laser-based thermal spectroscopy techniques, such as the thermoreflectance approach for measuring thermal boundary resistances and thermal conductivity of nanosized structures. When a material, for instance, a thin metal film, is irradiated by a short-pulsed laser, the electrons first absorb the deposited thermal energy from the laser and then transmit the energy to the lattice, eventually increasing the lattice temperature. This interaction will continue until electrons and

phonons reach their thermal equilibrium states, at which electron and lattice reach the same temperature.

A wide range of studies have been performed to understand thermal transport involving EPI in single and multi-layer thin films irradiated by short laser pulses. These include the pioneering research by Qiu et al. [12-15] in the early 1990s, in which heat transfer across thin films (e.g., single-layer Au, double-layer Au-Cr and triple-layer Au-Cr-Au films) under ultrafast laser heating was examined experimentally and theoretically. Specifically, the diffusive 2T model was employed to model the thermal interactions between electrons and phonons, and it was shown that this model can appropriately describe the transient heat conduction processes in thin films, matching well with experimental data. Later, the diffusive 2T model has shown to be effective in modeling, elucidating and predicting various electron-phonon coupled thermal transport problems in laser manufacturing or processing [16-19].

While the afore-discussed studies demonstrated the importance of considering EPI in thermal modeling of metal films under ultrafast laser irradiation, it has been well known that a Fourier's law-based model cannot accurately predict thermal transport in small-sized materials or under ultrafast thermal transients [20, 21], such as pico-/femto-second laser irradiation. Thus, recently, researchers have directed considerable efforts to improve the diffusive 2T model to elucidate the complex problems in practical applications. Chen et al. [22] presented a semiclassical 2T model by replacing the electron heat diffusion equation in the 2T model with the Boltzmann transport equation, which can model the electron drifting effect that is important in ultrafast laser heating scenarios. Poletkin et al. [23] replaced the phonon heat diffusion equation in the diffusive 2T model with the Cattaneo wave model. This eventually transforms the diffusive 2T model to a hyperbolic heat transfer model, which was shown to better model electron-phonon coupled thermal transport in Au films heated by ultrashort laser pulses than the diffusive 2T model. Similarly, Abouelrega modified the diffusive 2T model by modeling heat diffusion with a thermoelastic model containing two phase-lag terms [24]. The author also suggested that this model can be applied to study various problems, ranging from optics to material design and thermodynamics. Mittal and Kulkarni [25] combined the dual-phase-lag model and the 2T thermoelasticity theory based on the time-fractional approach and obtained some results for the spherical bounded domain, including thermal and hoop stresses, conductive and thermodynamic temperatures, and additionally studied the effects the variation in lagging times and fractional derivative order on the results obtained. The hyperbolic 2T model was presented to conduct the thermodynamic temperature of a semiconductor medium and it was mentioned that this model can take the finite velocity for the thermal and mechanical waves propagation into account through the medium [26]. Shen et al. [27] proposed the fractional form of 2T model to investigate the heat conduction in nanoscales caused by ultrafast laser heating of materials. Ho et al. [28] developed the diffusive 2T model using the dual-phase-lag theory to conduct the thermal transport in Au thin films of various thicknesses heated by short-pulsed laser.

Now it is well known that the thermal resistance at interfaces plays a vital role in the thermal transport, especially in multi-layer thin films, nanograined materials, nanocomposites, or aggregated micro/nanoparticles. Moreover, the electron-electron, phonon-phonon, and electron-

phonon interactions close to and across the interface of two metals or a metal and a nonmetal led to multiple, coupled thermal energy exchange channels, which all should be considered to accurately model heat transfer in materials containing dense interfaces or grain boundaries. There have been a wide range of research works utilizing different approaches, theoretically, computationally, or experimentally, to investigate those heat transfer channels, particularly those that differ from a direct phonon or electron transmission channel. Notably, Huberman [29] proposed a cross-interface inelastic electron-phonon coupling mechanism, which states that phonons in Pb and phonons in diamond can form a joint phonon mode, thus allowing direct thermal transport from phonons in diamond to electrons in Pb through EPI. Later, Sergeev [30] rigorously calculated the thermal conductance caused by cross-interface EPI via Green's functions. Costescu et al. [31] used the time-domain thermoreflectance method to calculate the interfacial thermal conductance for epitaxial TiN/crystal oxide at different temperatures, ranging from 79.4 to 294 K. Giri et al. [32] examined the electron-phonon coupling at the interface of metal/nonmetal film, suggesting that this heat transport channel can increase the interfacial heat dissipation rate, by which hot electrons in the metal can transmit thermal energy to the cool substrate phonons when the electrons and phonon are out of the thermal equilibrium state. The importance of this cross-interface inelastic EPI on thermal transport has been demonstrated in several laser pump-probe experiments [33-35]. Furthermore, the calculation of the interfacial thermal conductance for multilayered structures such as Cr/Si, Al/Cu and metal-GaN films was performed in Refs. [36-38]. Wang et al. [9] applied the 2T-MD simulation to explain the EPI in metal layer of the Cu/Si film and claimed that the 2T-MD method can capture the electron-phonon nonequilibrium near metal-nonmetal interface and studied its effect on hindering thermal transport. Lu et al. [11] further improved the 2T model to include cross -interface EPI and showed that this could be an important mechanism in certain cases. Wang et al. [10] showed that the 2T-BTE model can capture ballistic and quasi-ballistic transport behaviors of both electron and phonons, only needs parameters predicted from first principles, and can readily include EPI and phonon transmission and electron transmission. However, the limitation is in its high computational cost.

In this work, we propose a time-fractional form of the 2T (2T-TF) model to simulate the sub-diffusive thermal transport in multi-layer metal-nonmetal thin films heated by femtosecond laser pulses. The time derivative term in the electron thermal transport equation of the diffusive 2T model is replaced by a non-integer time-derivative term to take account of the anomalous diffusion of electronic thermal energy. Phonon transmission and electron transmission terms can also be readily implemented in the model. The numerical results of the proposed 2T-TF model will be compared to those of 2T-BTE presented in Ref. [10] and to available experimental data [15, 44], validating our model and demonstrating its lower computational cost than the 2T-BTE approach.

2. Mathematical formulations of the 2T-TF model

The diffusive form of the 2T model, in which the heat diffusion equations of electron and phonon are coupled through an electron-phonon coupling term can be written as,

$$C_e \frac{\partial T_e}{\partial t} = k_e \frac{\partial^2 T_e}{\partial x^2} - G\left(T_e - T_p\right) + S(x,t), \tag{1a}$$

$$C_p \frac{\partial T_p}{\partial t} = k_p \frac{\partial^2 T_p}{\partial x^2} + G\left(T_e - T_p\right) \tag{1b}$$

where T is the temperature, C is the volumetric heat capacity, k is the thermal conductivity, G is the electron-phonon coupling factor and S is the laser heating source. The subscripts e and p represent the electron and phonon channel, respectively. The diffusive 2T model has been employed to describe EPI in metallic films under laser irradiation or during electron-phonon coupled thermal transport across metal-nonmetal interfaces. It must be mentioned that in a typically nano-/pico-/femto-second laser heating process of thin films, the temporal and spatial scales could be on the order of nano-/pico-/femto-second and micro-/nano-meter, respectively, which are comparable to the relaxation time and MFP of heat carriers. The validity of Fourier's law for modeling electron-phonon coupled thermal transport in these regimes is thus questionable. Notably, anomalous diffusion processes have been observed in the electron temperature, indicating that the diffusive form of electron heat diffusion equation is no longer valid [4, 30]. Mozafarifard et al. [40, 41] presented a Caputo-type time-fractional heat conduction equation to examine the thermal interaction between laser pulses and thin metal films. They argued that due to the deviation between the results of Fourier model and experimental findings reported in Refs. [15, 44], the heat transfer mechanism in the laser heating of thin films cannot be explained by the diffusive heat conduction equation, suggesting that the fractional form of energy equation is needed for characterizing such processes. Specifically, the comparison between the results of Fourier's model and measured data showed remarkable disagreement, indicating anomalous diffusion effects in the ultrashort laser heating of thin metal films. In fact, in normal diffusion, the mean square displacement of particles linearly depends on time ($\langle x^2 \rangle \sim \alpha t$ where α is the constant diffusivity), whereas for the anomalous diffusion process, this relationship can be expressed by a power law ($\langle x^2 \rangle \sim \alpha(t) t^{\beta}$ where β is the anomalous diffusion exponent and $\alpha(t)$ is the time-dependent diffusivity which defined as $\alpha(t) \sim t^{\beta-1}$) [40].

Based on the discussion above, the fractional form of diffusive 2T model can be derived by the generalization of electron energy equation in Eq. (1), and replacing the time-derivative term with fractional derivative with non-integer order of β as,

$$C_e \frac{\partial^{\beta} T_e}{\partial t^{\beta}} = k_e \tau_e^{1-\beta} \frac{\partial^2 T_e}{\partial x^2} - G\left(T_e - T_p\right) + S(x,t), \tag{2a}$$

$$C_p \frac{\partial T_p}{\partial t} = k_p \frac{\partial^2 T_p}{\partial x^2} + G\left(T_e - T_p\right) \tag{2b}$$

where β is the order of fractional derivative, τ is the relaxation time and $\partial^{\beta} T_e / \partial t^{\beta}$ is the time-derivative term with non-integer order. When $\beta = 1$, the time-fractional electron energy equation reduces to the diffusive form, while when $\beta \neq 1$ the electron energy equation describes anomalous diffusion processes. In addition, τ_e is the electron relaxation time [4, 40]. This required finite time cannot be characterized by the diffusive form of heat energy equation, which is because the Fourier's law corresponds to infinite velocity in the space domain. In other words, in the Fourier's law-based diffusive 2T model, phonons can be instantly heated by hot electrons far away, which

is unphysical. Thus, the fractional form of electron heat diffusion proposed in Eq. (2a) is more appropriate to model electronic thermal transport.

The laser heating source term in the Eq. (2) can be represented based on the Gaussian profile [39]:

$$S(x,t) = \sqrt{\frac{\mu}{\pi}} \frac{(1-R)}{t_p(\delta_s+\delta_b)\left[1-exp\left(\frac{-L}{\delta_s+\delta_b}\right)\right]} I_0\, exp\left[-\frac{x}{(\delta_s+\delta_b)} - \mu\left(\frac{t-2t_p}{t_p}\right)^2\right] \quad (3)$$

where R is the surface reflectivity to the laser irradiation, δ_s is the optical penetration depth, δ_b is the ballistic length of electron, t_p is the laser pulse duration, I_0 is the laser fluence, L is the thickness of the top metallic layer and $\mu = 4\ln(2)$.

In this work, we use Au thin film/Si substrate and Au thin film/thin Al or Pt interlayer/Si substrate as model system, as schematically illustrated in Figs. (1a) and (1b) respectively. As shown in Fig. (1a), for the Au/Si film without interlayer, hot electrons in Au must first transfer their energy to Au phonons via EPI (depicted by the G parameter) and then via phonon transmission (depicted by the phonon interfacial thermal resistance, R_{pp}). After inserting an interlayer between the Au thin film and Si substrate, as shown in Fig. (1b), additional thermal transport channels are created. The phonon transmissions at the interfaces of Au film, interlayer and Si substrate characterized by the phonon thermal resistances R_{pp} significantly affect the thermal transport in multilayered thin films. Additionally, the electron transmission at the Au/interlayer interface is another important heat dissipation channel caused by the energy exchange between electrons of Au and interlayer, of which the resistance is quantified by R_{ee}.

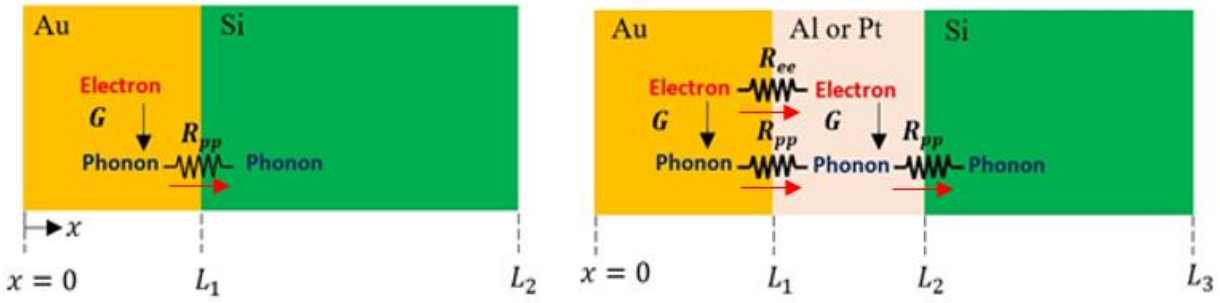

Fig. 1. The schematics of (a) Au/Si film without interlayer, and (b) Au/Si film with an interlayer.

At the Au/interlayer (Al or Pt) interface, we have two thermal boundary resistances, including the electron thermal resistance $R_{ee,AuAl}$ and the phonon thermal resistance $R_{pp,AuAl}$. In addition, at the interface of interlayer and Si substrate, we have the phonon thermal resistance of $R_{pp,AlSi}$ [10]. Finally, EPI inside the Au thin film and metallic interlayer (Al or Pt) allows heat transfer from hot electrons to the lattice. Considering all the interfacial heat transfer pathways mentioned above, we apply the following boundary conditions to the case of Au/Si structure without interlayer. Adiabatic boundary conditions are applied to both the phonon and electron channels at the left boundary ($x = 0$) and right boundary ($x = L_2$) of the Au/Si structure.

$$\left.\frac{\partial T_{e,Au}}{\partial x}\right|_{x=0} = 0, \tag{4a}$$

$$\left.\frac{\partial T_{p,Au}}{\partial x}\right|_{x=0} = 0, \tag{4b}$$

$$-k_{p,Au}\left.\frac{\partial T_{p,Au}}{\partial x}\right|_{x=L_1} = \left.\frac{T_{p,Au} - T_{p,Si}}{R_{pp,AuSi}}\right|_{x=L_1}, \tag{4c}$$

$$-k_{p,Si}\left.\frac{\partial T_{p,Si}}{\partial x}\right|_{x=L_1} = \left.\frac{T_{p,Au} - T_{p,Si}}{R_{pp,AuSi}}\right|_{x=L_1}, \tag{4d}$$

$$\left.\frac{\partial T_{e,Au}}{\partial x}\right|_{x=L_1} = 0, \tag{4e}$$

$$\left.\frac{\partial T_{p,Si}}{\partial x}\right|_{x=L_2} = 0 \tag{4f}$$

and also, for Au/Si film with an interlayer (subscript $Int.$), we have:

$$\left.\frac{\partial T_{e,Au}}{\partial x}\right|_{x=0} = 0, \tag{5a}$$

$$\left.\frac{\partial T_{p,Au}}{\partial x}\right|_{x=0} = 0, \tag{5b}$$

$$-k_{e,Au}\left.\frac{\partial T_{e,Au}}{\partial x}\right|_{x=L_1} = \left.\frac{T_{e,Au} - T_{e,Int.}}{R_{ee,AuInt.}}\right|_{x=L_1}, \tag{5c}$$

$$-k_{p,Au}\left.\frac{\partial T_{p,Au}}{\partial x}\right|_{x=L_1} = \left.\frac{T_{p,Au} - T_{p,Int.}}{R_{pp,AuInt.}}\right|_{x=L_1}, \tag{5d}$$

$$-k_{e,Int.}\left.\frac{\partial T_{e,Int.}}{\partial x}\right|_{x=L_1} = \left.\frac{T_{e,Au} - T_{e,Int.}}{R_{ee,AuInt.}}\right|_{x=L_1}, \tag{5e}$$

$$-k_{p,Int.}\left.\frac{\partial T_{p,Int.}}{\partial x}\right|_{x=L_1} = \left.\frac{T_{p,Au} - T_{p,Int.}}{R_{pp,AuInt.}}\right|_{x=L_1}, \tag{5f}$$

$$\left.\frac{\partial T_{e,Int.}}{\partial x}\right|_{x=L_2} = 0, \tag{5g}$$

$$-k_{p,Int.}\left.\frac{\partial T_{p,Int.}}{\partial x}\right|_{x=L_2} = \left.\frac{T_{p,Int.} - T_{p,Si}}{R_{pp,Int.Si}}\right|_{x=L_2}, \tag{5h}$$

$$-k_{p,Si}\left.\frac{\partial T_{p,Si}}{\partial x}\right|_{x=L_2} = \left.\frac{T_{p,Int.} - T_{p,Si}}{R_{pp,Int.Si}}\right|_{x=L_2}, \tag{5i}$$

$$\left.\frac{\partial T_{p,Si}}{\partial x}\right|_{x=L_3} = 0 \tag{5j}$$

Eqs. (4) and (5) defined above provide the complete boundary conditions to solve the 2T-TF model, Eq. (2). It is worth noting that we only model the phonon thermal transport channel in the Si substrate, because electronic thermal transport is negligible in pure or lightly doped silicon.

Finally, the initial conditions required to solve the Eq. (2) are,

$$T_e(x,0) = T_p(x,0) = T_0 = 300 \text{ K} \tag{6}$$

which indicates that before laser irradiation, the Au top layer, Si substrate and interlayer (Al or Pt) are all initially at room temperature.

3. Numerical Implementation

In this section, we present the numerical approach based on the finite difference method to solve the 2T-TF model discussed in Section (2). For the time-derivative term with fractional order of β, the Caputo derivative definition is employed [42]. The electron energy equation is implicitly discretized, and an explicit scheme is applied to discretize the phonon energy equation. In addition, Thomas's algorithm is employed to arrange the tridiagonal matrix related to the electron energy equation.

3.1. Phonon thermal transport equation

The first-order time-derivative and the second-order space-derivative terms in the phonon energy equation, Eq. (2b), are discretized based on the backward and central differencing as,

$$\left(\frac{\partial^2 T_p}{\partial x^2}\right)_{i,n} = \frac{T_{p,i+1}^{n-1} - 2T_{p,i}^{n-1} + T_{p,i-1}^{n-1}}{(\Delta x)^2} + \mathcal{O}(\Delta x^2), \tag{7a}$$

$$\left(\frac{\partial T_p}{\partial t}\right)_{i,n} = \frac{T_{p,i}^{n} - T_{p,i}^{n-1}}{\Delta t} + \mathcal{O}(\Delta t) \tag{7b}$$

where subscripts i and n indicate the spatial and temporal steps in the computational domain. Inserting Eqs. (7a) and (7b) into Eq. (2b) gives:

$$\frac{C_p}{\Delta t}\left(T_{p,i}^{n} - T_{p,i}^{n-1}\right) = \frac{k_p}{\Delta x^2}\left(T_{p,i+1}^{n-1} - 2T_{p,i}^{n-1} + T_{p,i-1}^{n-1}\right) + G\left(T_{e,i}^{n-1} - T_{p,i}^{n-1}\right) \tag{8}$$

Upon arranging Eq. (8), the explicitly discretized form of the phonon energy equation, Eq. (2b), can be rewritten in the following form:

$$T_{p,i}^{n} = \left[1 - \frac{2k_p}{\Delta x^2}\frac{\Delta t}{C_p} - \frac{G\Delta t}{C_p}\right] T_{p,i}^{n-1} + \left[\frac{k_p}{\Delta x^2}\frac{\Delta t}{C_p}\right]\left(T_{p,i+1}^{n-1} + T_{p,i-1}^{n-1}\right) + \left[\frac{G\Delta t}{C_p}\right] T_{e,i}^{n-1} \tag{9}$$

For the stability of the numerical solution of Eq. (9), the mesh steps Δt and Δx are 0.4 fs and 0.5 nm, taking into account that the coefficient of $T_{p,i}^{n-1}$, $\left[1 - 2k_p\Delta t/\Delta x^2\, C_p -\right.$

$G\Delta t/C_p\big]$, must be greater than zero so as to provide convergence for the numerical solutions. Eq. (9) is used to determine the phonon temperature in the Au top layer, Si substrate and the interlayer of Al or Pt. It also must be mentioned that for the Si substrate, the electron-phonon coupling factor is zero, due to the lack of free electrons in the dielectric materials, as a result the terms consisting of G would be removed from the phonon energy equation. Therefore, the Eq. (9) can be rewritten for the Si substrate as,

$$T_{p,i}^{n} = \left[1 - \frac{2k_p}{\Delta x^2}\frac{\Delta t}{C_p}\right] T_{p,i}^{n-1} + \left[\frac{k_p}{\Delta x^2}\frac{\Delta t}{C_p}\right]\left(T_{p,i+1}^{n-1} + T_{p,i-1}^{n-1}\right) \tag{10}$$

Similarly, the coefficient of $T_{p,i}^{n-1}$, $\left[1 - 2k_p\Delta t/\Delta x^2\, C_p\right]$, must be greater than zero to guarantee the stability of numerical solution of Eq. (10).

3.2. Electron thermal transport equation

The time-derivative term with fractional order in Eq. (2a) is defined based on the numerical approximation of Caputo's definition as [40],

$$\frac{\partial^\beta T_e}{\partial t^\beta} = \sigma_\beta \sum_{j=1}^{n} \omega_j^\beta \left(T_{e,i}^{n-j+1} - T_{e,i}^{n-j}\right) \tag{11}$$

where ω_j^β is the weighted arithmetic mean and σ_β is the fractional factor which are defined by following relationships [40]:

$$\omega_j^\beta = \left[j^{1-\beta} - (j-1)^{1-\beta}\right], \tag{12a}$$

$$\sigma_\beta = \frac{1}{(1-\beta)\Delta t^\beta \Gamma(1-\beta)} \tag{12b}$$

Further details of deriving the numerical formulations of the Caputo fractional derivative can be found in Ref. [40]. The second-order space differentiation in Eq. (2a) can be approximated by the central difference scheme as

$$\left(\frac{\partial^2 T_e}{\partial x^2}\right)_{i,n} = \frac{T_{e,i+1}^{n} - 2T_{e,i}^{n} + T_{e,i-1}^{n}}{(\Delta x)^2} + \mathcal{O}(\Delta x^2) \tag{13}$$

Putting the Eqs. (11) and (13) into Eq. (2a), the implicitly discretized form of time-fractional electron energy equation can be derived as,

$$C_e\sigma_\beta \sum_{j=1}^{n} \omega_j^\beta \left(T_{e,i}^{n-j+1} - T_{e,i}^{n-j}\right) = \frac{k_e \tau_e^{1-\beta}}{\Delta x^2}\left(T_{e,i+1}^{n} - 2T_{e,i}^{n} + T_{e,i-1}^{n}\right) - G\left(T_{e,i}^{n} - T_{p,i}^{n}\right) + S(i,n) \tag{14}$$

The first term in the fractional derivative series should be separated to implement the implicit scheme for the numerical solution of electron thermal transport equation:

$$C_e\sigma_\beta\left(T_{e,i}^n - T_{e,i}^{n-1}\right) + C_e\sigma_\beta \sum_{j=2}^{n} \omega_j^\beta \left(T_{e,i}^{n-j+1} - T_{e,i}^{n-j}\right) = \frac{k_e \tau_e^{1-\beta}}{\Delta x^2}\left(T_{e,i+1}^n - 2T_{e,i}^n + T_{e,i-1}^n\right) - G\left(T_{e,i}^n - T_{p,i}^n\right) + S(i,n) \quad (15)$$

Then, arranging Eq. (15) gives the discretized form of Eq. (2a) as:

$$\left[\frac{k_e \tau_e^{1-\beta}}{\Delta x^2}\right] T_{e,i-1}^n - \left[\frac{2k_e \tau_e^{1-\beta}}{\Delta x^2} + C_e\sigma_\beta + G\right] T_{e,i}^n + \left[\frac{k_e \tau_e^{1-\beta}}{\Delta x^2}\right] T_{e,i+1}^n = -C_e\sigma_\beta T_{e,i}^{n-1} + C_e\sigma_\beta \sum_{j=2}^{n} \omega_j^\beta \left(T_{e,i}^{n-j+1} - T_{e,i}^{n-j}\right) - GT_{p,i}^n - S(i,n) \quad (16)$$

Eq. (16) represents the discretized form of the Caputo-type time-fractional electron thermal transport equation based on an implicit scheme, and it has been used to calculate the electron temperatures in the Au top layer and the metallic interlayer. The space and time steps are the same as before, $\Delta t = 0.4\ fs$ and $\Delta x = 0.5$ nm, to satisfy the mesh independence of numerical solutions from the mesh grid. The electron heat capacity is taken as a parameter dependent on the electron temperature based on the linear relationship $C_e(T_e) = \gamma_e T_e$ [10, 36], where γ_e is the electron heat capacity constant. This linear relationship based on the Sommerfeld expansion can provide sufficient details about the electron heat capacity, in particular for the low electron temperature regime [43]. The main reason to employ an implicit scheme to solve Eq. (16) is the dependence of electronic heat capacity on electron temperature and σ_β on the order of fractional derivative, respectively. In numerical solution of Eq. (16), the value of electronic heat capacity is often changing because it depends on electron temperature based on the Sommerfeld expansion, and the fractional parameter σ_β, Eq. (12b), depends on the value of order of fractional derivative β, rendering it challenging to choose a specific value for Δt. Moreover, the term Δt^β in Eq. (12b) can change due to different values of β. Therefore, it is challenging to use the explicit scheme to numerically solve the electron thermal transport equation because any change in value of electronic heat capacity and fractional parameter can affect the stability condition, so the implicit scheme is the most effective and straightforward approach to address those challenges.

The coupled Eqs. (9), (10) and (16) will be solved simultaneously to calculate the phonon temperatures of Au, interlayer (Al or Pt) and Si substrate, and the electron temperatures of Au and interlayer (Al or Pt), considering the boundary conditions, Eqs. (4) and (5), to model thermal transport across metal/metal/dielectric and metal/dielectric films.

4. Results and discussion

In this section, we will present the numerical results of our 2T-TF model and compare them to experimental data [15, 44], 2T-BTE data Ref. [10], and results of the diffusive 2T model. The materials properties used in our models are presented in Table (1).

Table 1. The thermophysical properties of different materials.

Properties	Au	Al	Pt	Si
k_e (W/mK)[a]	311.4	199.5	65.8	N/A
k_p (W/mK)[a]	2.6	5.5	5.8	148.0
C_p ($\times 10^6$ J/m^{3}K)[a]	2.4	2.43	2.67	1.66
γ_e ($\times 10^6$ W/m^{3}K^2)[b]	62.9	91.2	748.1	N/A
τ_e (ps)[c]	0.7438	0.1099	0.1904	N/A
G ($\times 10^{16}$ W/m^{3}K)[b]	2.6	24.6	108.7	N/A

[a] Wang et al. [10], [b] Lin and Zhigilei [43], [c] Tzou [15, 44].

A variety of approaches can be used to obtain, experimentally or theoretically, the thermophysical properties needed for thermal modeling. In addition to the conventional approaches for obtaining thermal conductivity of bulk materials, pump-probe thermoreflectance methods (e.g., TDTR and FDTR) have been extensively used to obtain thermal conductivity and interfacial thermal resistance of materials [45]. On the other hand, first-principles methods and classical atomistic methods (like molecular dynamics) can be applied to obtain the thermophysical properties of materials such as thermal conductivities, heat capacities, and electron-phonon coupling factor. Refs. [46-49] have reported or discussed how we can calculate thermal conductivity, heat capacity, electron-phonon coupling factor, relaxation time, group velocity, and other properties for metals and nonmetals.

4.1. Fitting of the 2T-TF model to experimental data

In Refs. [15, 50], the thermal transport of the single-layer Au films with different thicknesses was experimentally studied, and the normalized electron evolutions at the front surface of film, $x = 0$, defined based on the relationship below,

$$T_{e,normalized} = [T_e(0,t) - T_0]/[T_{e,max} - T_0] \quad (17)$$

were reported with respect to the time. The T_0 is the initial temperature which is equal to 300 K and $T_{e,max}$ is the maximum temperature of electrons during the laser heating of Au samples. The model parameters for Gaussian laser pulse are the same as Ref. [13], in which $R = 0.93$, $I_0 = 13.4$ J/m^2, and $\delta_s = 15.3$ nm. The laser pulse duration is $t_p = 100$ fs for Au films with thicknesses of 20 and 100 nm (Fig. (2a)) [13], but for Au sample of thickness 200 nm, the laser pulse duration is taken as $t_p = 96$ fs (Fig. (2b)) [50] to produce the same laser heating as that during the experiments.

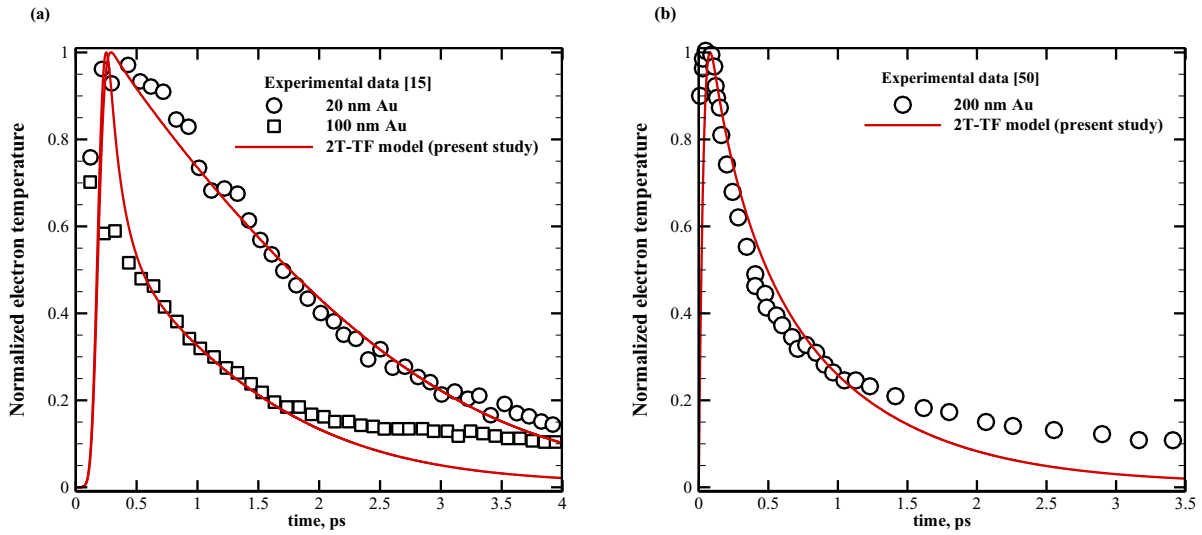

Fig. 2. Comparison between experimental data and results of 2T-TF for single-layer Au films.

The comparison in Fig. (2) highlights the ability of 2T-TF model proposed in this study to reasonably fit experimental curves. For single-layer Au film, the only interaction between heat carriers is the thermal transport from hot electrons to the cool phonons, by which the energy absorbed from the laser source would be transmitted to the phonons in the Au layer by the hot electrons through EPI. Moreover, Fig. (2) clearly demonstrates the effect of Au layer thickness on the normalized electron temperature: the electron temperature declines more rapidly in the thicker film than the thinner film. This is because the heated electrons can quickly move away from the surface of the thicker samples, which is a well-known phenomenon in laser pump-probe experiments on thick metallic films.

Finally, we point out that $\beta = 0.99$ was used in our 2T-TF model in Fig. 2, which corresponds to almost entirely diffusive thermal transport, because the 2T-TF equations in Eq. (2) reduce to the diffusive heat equations in Eq. (1) when $\beta \approx 1$. Obviously, the diffusive heat transfer model suffices to model the evolution of electron temperature when EPI dominates. This explains why earlier studies adopting the diffusive 2T model based on the Fourier's law can well fit and predict many pump-probe experimental data even without using a more sophisticated model [51, 52]. However, as discussed below, it is important to use a non-Fourier transport model when there is interfacial thermal transport between different nanosized components.

4.2. Detailed comparison between the diffusive 2T model with the 2T-TF model

Here, we performed a detailed comparison between the diffusive 2T model and the 2T-TF model. First, we will use the well-established diffusive 2T model to validate our 2T-TF model, because mathematically the newer model should approach that of the diffusive model when $\beta \approx 1$. As shown in Fig. (3), the results of 2T-TF model for $\beta = 0.99$ agree with those from the diffusive 2T model, directly confirming the equivalence of these two models in the diffusive transport regime. Specifically, 2T-TF model and the diffusive model predict similar electron and

phonon temperatures during laser heating of Au thin film. The fast and significant rise in electron temperature is because of the direct absorption of laser energy by electrons, while the lagged and milder increase in phonon temperature is because of the weak EPI in Au and the much larger heat capacity of phonons than electrons.

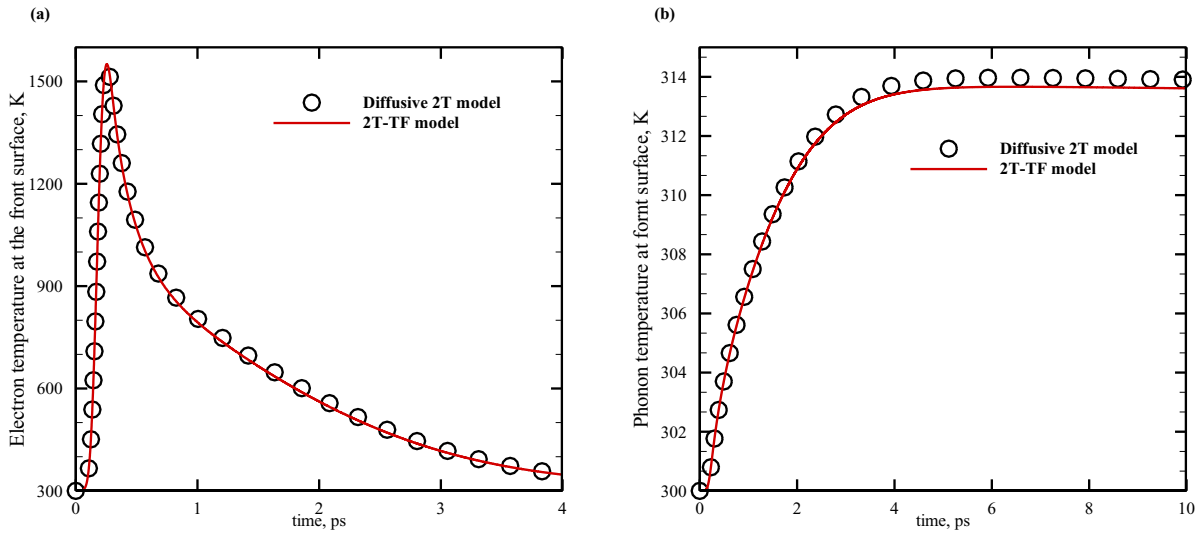

Fig. 3. Comparison between the results of 2T-TF and diffusive 2T models for thermal transport in a 100-nm Au thin film. (a) Electron temperature evolution, (b) Phonon temperature evolution.

In Fig. (4) we present the results of 2T-TF model for different values of fractional derivative order β for a 100-nm single-layer Au film, which are compared against those from the diffusive 2T model. As expected, for smaller values of β, there would a larger deviation between the two models, because the diffusive model cannot capture the stronger non-diffusive heat transfer process as captured by the 2T-TF with smaller β. Moreover, the non-diffusive transfer behavior affects both the evolution of electron temperature and phonon temperature significantly, indicating the importance to consider it in relevant processes, such as ultrafast laser manufacturing of nanopowders or thermal modelling of nanosized heat-generating devices.

A more detailed comparison between different curves (for $\beta = 0.9, 0.7, 0.5$ and 0.3) of the 2T-TF model in Fig. (4a) reveals that a reduced value of β leads to much fast decay in electron temperature. In Fig. (4a), the electron temperature follows an exponentially decaying trend, and the faster decline can be observed when the value of β decreases. In contrast, as shown in Fig. (4b), the phonon temperature would rise more quickly when the value of β decreases. The above observations mean that in 2T-TF models with reduced value of β, where heat transfer is faster than the diffusive limit, electrons can spread out the absorbed thermal energy deeper into the film more quickly, leading to a larger volume for EPI, and thus accelerating the loss of electronic thermal energy into phonons.

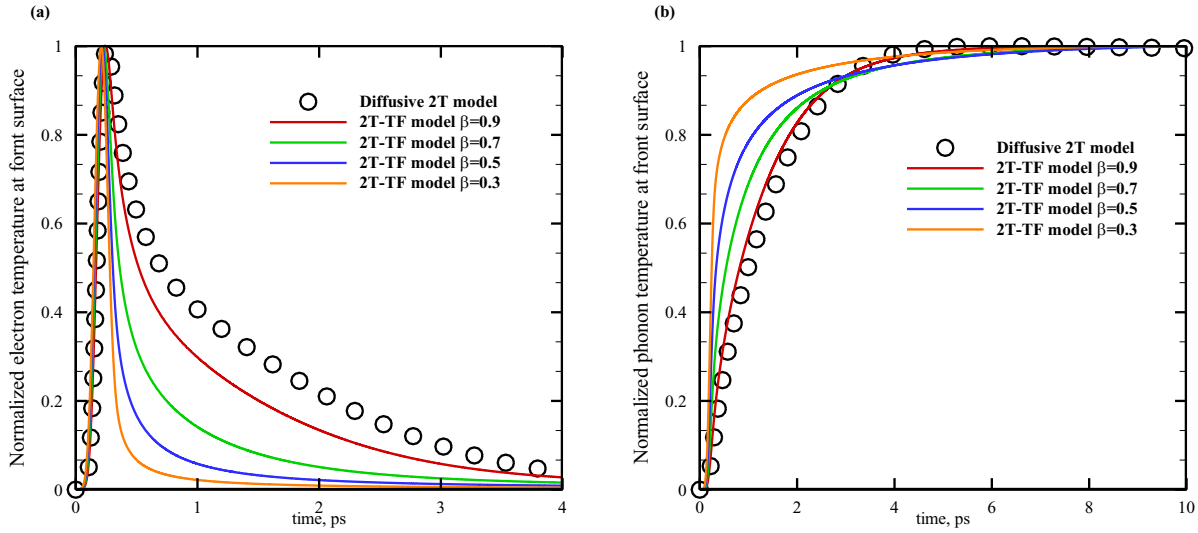

Fig. 4. The results of 2T-TF model for thermal transport in a 100-nm Au thin film for various values of β.

In addition to the single-layer Au films discussed above, we will compare between the 2T-TF model and the diffusive 2T model for laser heating of an Au thin film supported on a Si substrate, which serves as a simple model system of many electronic devices (which contains semiconductors and metals) and the case of laser processing of metal nanoparticles/powders on dielectric substrates. The same laser parameters as those used for Fig. (4) are used in these simulations on the Au/Si structure. Fig. (5) shows the electron temperature at the front surface of the Au layer, where the thicknesses of Au and Si substrate are 20 and 100 nm respectively. The agreement between the results of the 2T-TF model at $\beta = 0.99$ and those of the diffusive 2T model further confirms that the 2T-TF is at least valid and accurate in describing the diffusive limit of thermal transport.

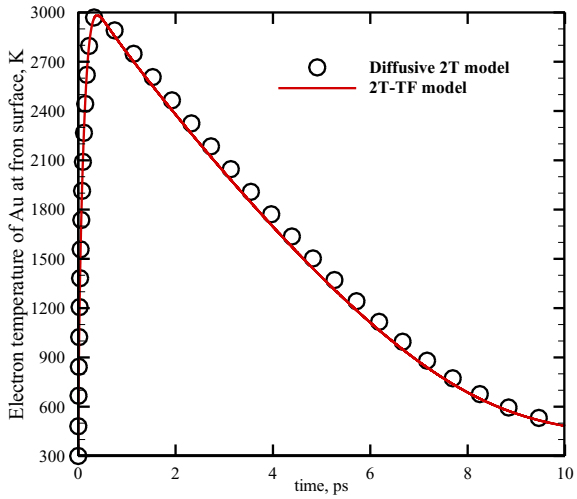

Fig. 5. Electron temperature evolution in the Au top layer of a 20-nm Au film/100-nm Si substrate heterostructure.

In addition, the evolution of phonon temperature at different locations of the Au/Si system is presented in Fig. (6a) and (6b). Specifically, Fig. (6a) highlights the phonon temperature at the top and rear surfaces of the Au thin film. The initial increase in phonon temperature is caused by the absorption of heat from the electrons through EPI, which occurs in a few picoseconds. The decreasing trend is because the heated phonons in the Au top layer can transmit their thermal energy to the Si substrate through the interfacial phonon transmission mechanism implemented in the 2T-TF model. On the other hand, Fig. (6b) shows the phonon temperature at the front and rear surface of the silicon substrate, both demonstrating an increasing trend with time. This is simply because of the transmission of phonon energy from the heated Au thin film. Finally, we emphasize that the phonon temperatures predicted by the 2T-TF model, in which $\beta = 0.99$, matches with the diffusive 2T model well, which again confirms the validity of the 2T-TF model in the diffusive regime.

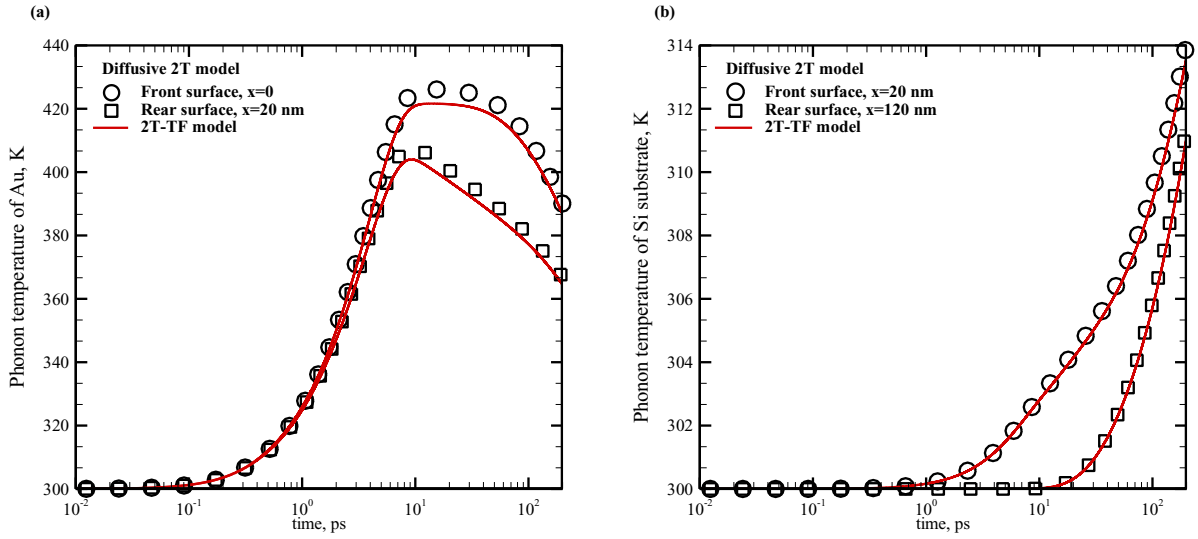

Fig. 6. Phonon temperature evolution in (a) the Au top layer and (b) the Si substrate of a 20-nm Au film/100-nm Si substrate heterostructure.

Furthermore, we analyze the effect of non-diffusive thermal transport on the thermal transients in the Au/Si structure under ultrafast laser heating, which will be achieved by adjusting the value of β. As shown in Fig. (7), the electron and phonon temperature in both the Au thin film and the Si substrate evolve in a dramatically different manner from the temperature evolution in a fully diffusive system (as predicted by the diffusive 2T model). This again emphasizes the importance of rigorously incorporating any non-diffusive transport mechanisms in the model for reliable thermal modeling of ultrafast thermal transport processes in nanosized systems. As shown in Fig. 7(a), similar to the case of single-layer thin films, as was presented in Fig. (4), the electron temperature decays faster when electronic thermal transport is more sub-diffusive (i.e., β

decreases). As a result, the electrons in the Au thin film cools down faster as β decreases, because the electronic heat can transfer faster to the rear end of the Au film, enlarging the interaction volume between electrons and phonons. However, the evolution of phonon temperature in the Au film depends on β differently for the Au/Si system, as presented in Fig. (7b), and the single-layer Au film, as presented in Fig. (4b). In Fig. (4b), the phonon temperature rises faster when β decreases, while Fig. (7b) shows an opposite trend. Specifically, the phonon temperature of the Au thin film rises more slowly and reaches a lower maximum temperature for smaller values of β. The primary reason for these different behaviors of phonon temperature in the single-layer Au film and the Au/Si system is the existence of a Si substrate in the latter.

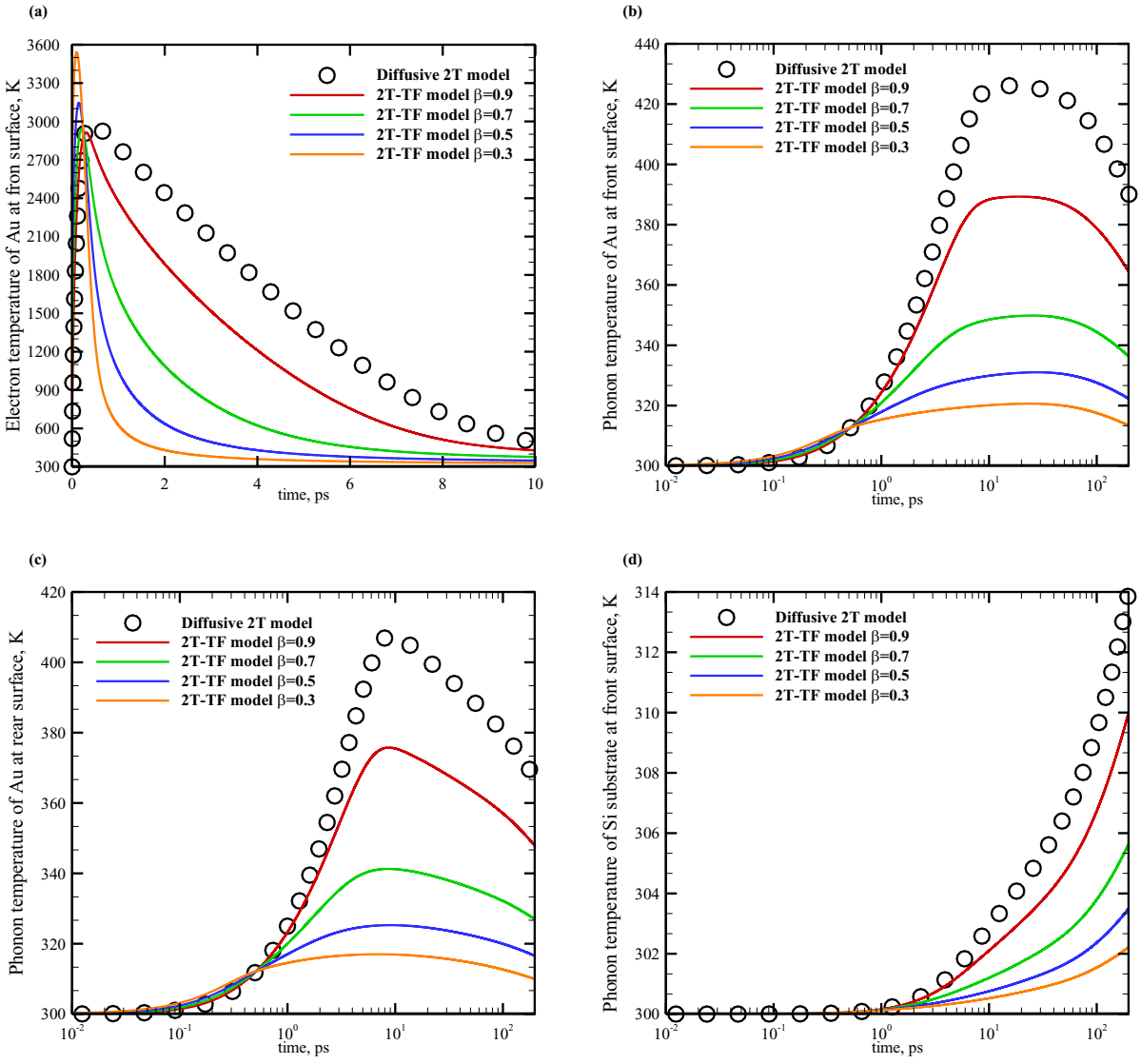

Fig. 7. Electron and phonon temperature evolution predicted by the 2T-TF model with different values of β (lines of different colors) for a 20-nm Au film/100-nm Si substrate heterostructure, as compared to the results from the diffusive 2T model (circles).

4.3. Boltzmann transport equation (BTE)

In this section, we will compare our 2T-TF model with the 2T-BTE model, which is the state-of-the-art thermal transport model that can consider ballistic to diffusive transport rigorously. Notably, Wang et al. [10] investigated the thermal transport behaviors in multi-layer metal/dielectric thin films under femtosecond laser irradiation using a 2T-BTE model. Their 2T-BTE model can capture the ballistic or quasi-ballistic effects in the laser heating of thin films, particularly when the thickness of the top Au layer is comparable to the MFPs of heat carriers. Here, we will compare the results of our 2T-TF model with the 2T-BTE results presented in Ref. [10], to demonstrate the capability of the 2T-TF model in capturing various thermal transport behaviors in multilayered metal/nonmetal heterostructures. The same thermophysical properties of Au, Al, Pt and Si as used in Ref. [10] are used in our 2T-TF modeling, as presented in Table (1). The thickness of Au top layer, interlayer and Si substrate are $20, 10$ and 100 nm respectively.

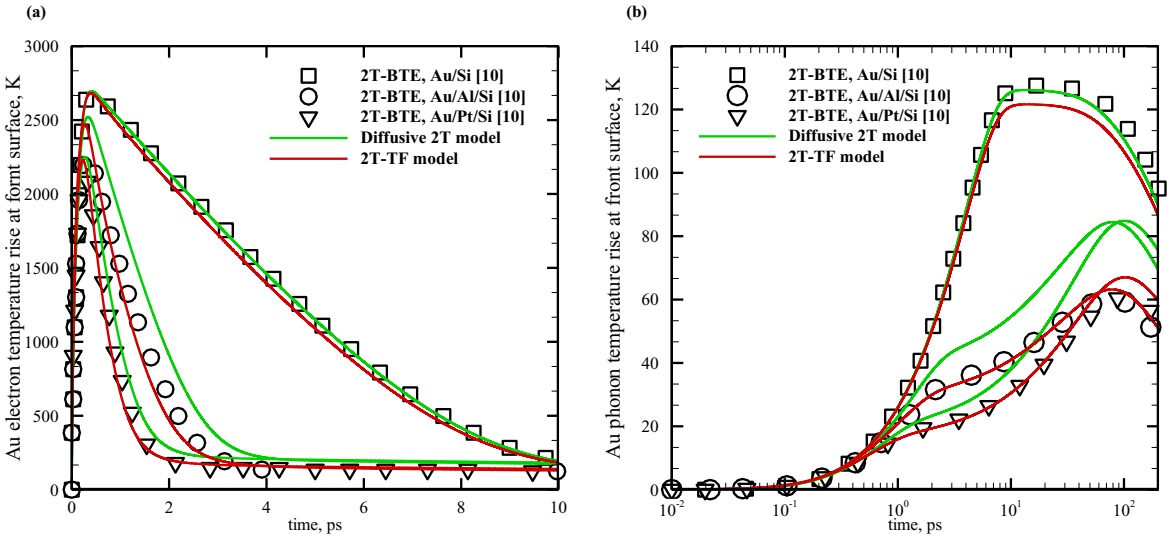

Fig. 8. Comparison between the results of the diffusive 2T model, the 2T-TF model, and the 2T-BTE model for thermal transport in 20-nm Au film/100-nm Si substrate and 20-nm Au film/10-nm Al or Pt interlayer/100-nm Si substrate heterostructures. (a) Electron temperature evolution at the front surface of the Au top film and (b) Phonon temperature evolution at the front surface of the Au top film.

Fig. (8) compares the results of the diffusive 2T, 2T-TF, and 2T-BTE models, specifically, for the electron and phonon temperatures at the front surface of the top Au layer. Obviously, the 2T-TF results can match with the 2T-BTE results significantly better than the diffusive 2T model. As shown in Figs. (8a) and (8b), the results of the diffusive 2T model are in rather good agreement with the 2T-BTE results in the Au/Si heterostructure without an interlayer. Even so, this does not mean that a thermal transport is indeed diffusive in the 20-nm-thick top layer. In fact, like the case

of Au single layer discussed earlier in the manuscript (Fig. 2), both the diffusive model and non-diffusive model can predict a rather flat (or uniform) electron temperature profile across the Au layer, because of the high thermal conductivity of electrons and, microscopically, the long electron MFP. However, the ballistic transport behavior of electrons begins to manifest itself after a metallic interlayer is inserted between the Au top layer and Si substrate. As shown in Fig. (8a) and (8b), the diffusive 2T model deviates significantly from the 2T-BTE results (circles and triangles) when there is an Al or Pt interlayer at the interface of Au and Si. The reason is because the interlayer allows the significant transmission of electrons into it, changing the previous adiabatic boundary condition for electron thermal transport at the rear surface of the Au top layer to a transmittable boundary condition. As a result, electrons in the non-diffusive models (both 2T-BTE and 2T-TF) can transmit faster into the interlayer than those modeled in the diffusive model. Thus, the electron temperature in the Au top layer predicted by 2T-BTE and 2T-TF drops faster than that predicted in the diffusive 2T model. Accordingly, the phonon temperature, which is directly affected by electron temperature through EPI inside the top layer, would increase more slowly in the 2T-BTE and 2T-TF models, because of the lower electron temperature, than what is predicted in the diffusive 2T model. Notably, β=0.9 was used in the 2T-TF model, indicating moderate ballistic (i.e., quasi-ballistic) transport characteristics of the system. This again confirms the importance of including non-diffusive phonon transport processes in a serious thermal transport model, even though its significance might be overlooked for systems with certain unique boundary conditions (like adiabatic boundary conditions for materials with high thermal conductivity).

Fig. (9) shows phonon temperature inside the interlayer of the Au/Al/Si and Au/Pt/Si heterostructures predicted from the diffusive 2T model, our 2T-TF model, and the 2T-BTE model. As predicted by all the models, the phonon temperature of interlayer first increases due to the transmission of hot phonons from the Au top layer and the transfer of thermal energy from hot electrons to phonons inside the interlayer, and then decreases due to the dissipation of heat to the cooler phonons in the Si substrate. However, the diffusive 2T model overestimates the phonon temperature. The reason for this is that the phonon temperature in Au top layer is higher predicted by the diffusive 2T model, meaning that the phonon transmission is much more significant in this model thus leading to hotter phonons in the interlayer. The results of 2T-TF model with order of fractional derivative $\beta = 0.9$ are well coincided with 2T-BTE simulations, which further highlights its capability of accurately modeling thermal transport in nano-/micro-sized heterostructures under ultrafast laser irradiation. The value of 0.9 for β again highlights that there is certain non-diffusive thermal transport process in the nanosized heterostructure studied here, which demands non-Fourier models like our 2T-TF model and 2T-BTE.

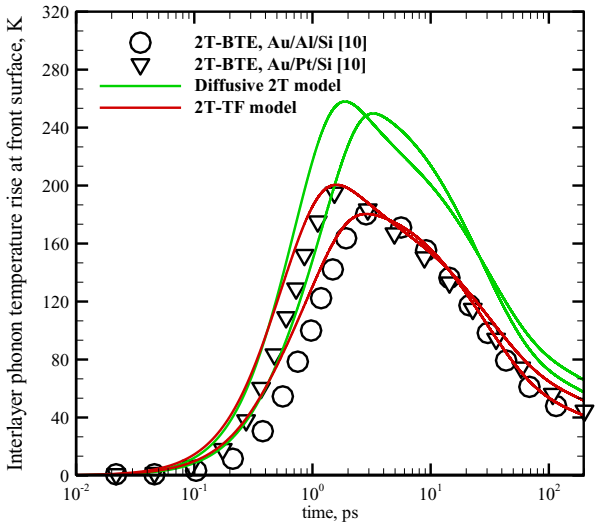

Fig. 9. Phonon temperature evolution at the front surface of the interlayer of a 20-nm Au film/10-nm Al or Pt interlayer/100-nm Si substrate heterostructure. Circles and triangles: 2T-BTE results. Green curve: the diffusive 2T model. Red curve: the 2T-TF model.

Next, we perform more detailed comparisons between the performance of diffusive 2T, 2T-TF, and 2T-BTE models by investigating Au/Al/Si heterostructures with different Au layer thicknesses. In Fig. 10, we present the electron and phonon temperature evolutions in Au/Al/Si heterostructures with 10-nm, 50-nm, and 200-nm-thick Au top layer. Apparently, the 2T-TF model can well match with 2T-BTE results, but the diffusive 2T model shows significant deviation from the other two models, particularly when the Au top layer is thin.

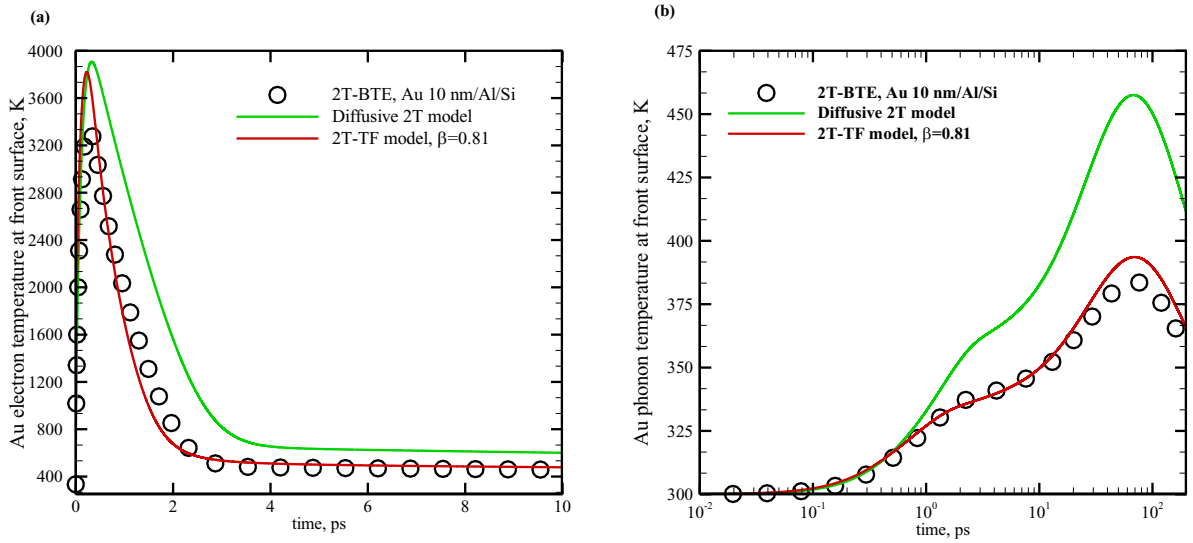

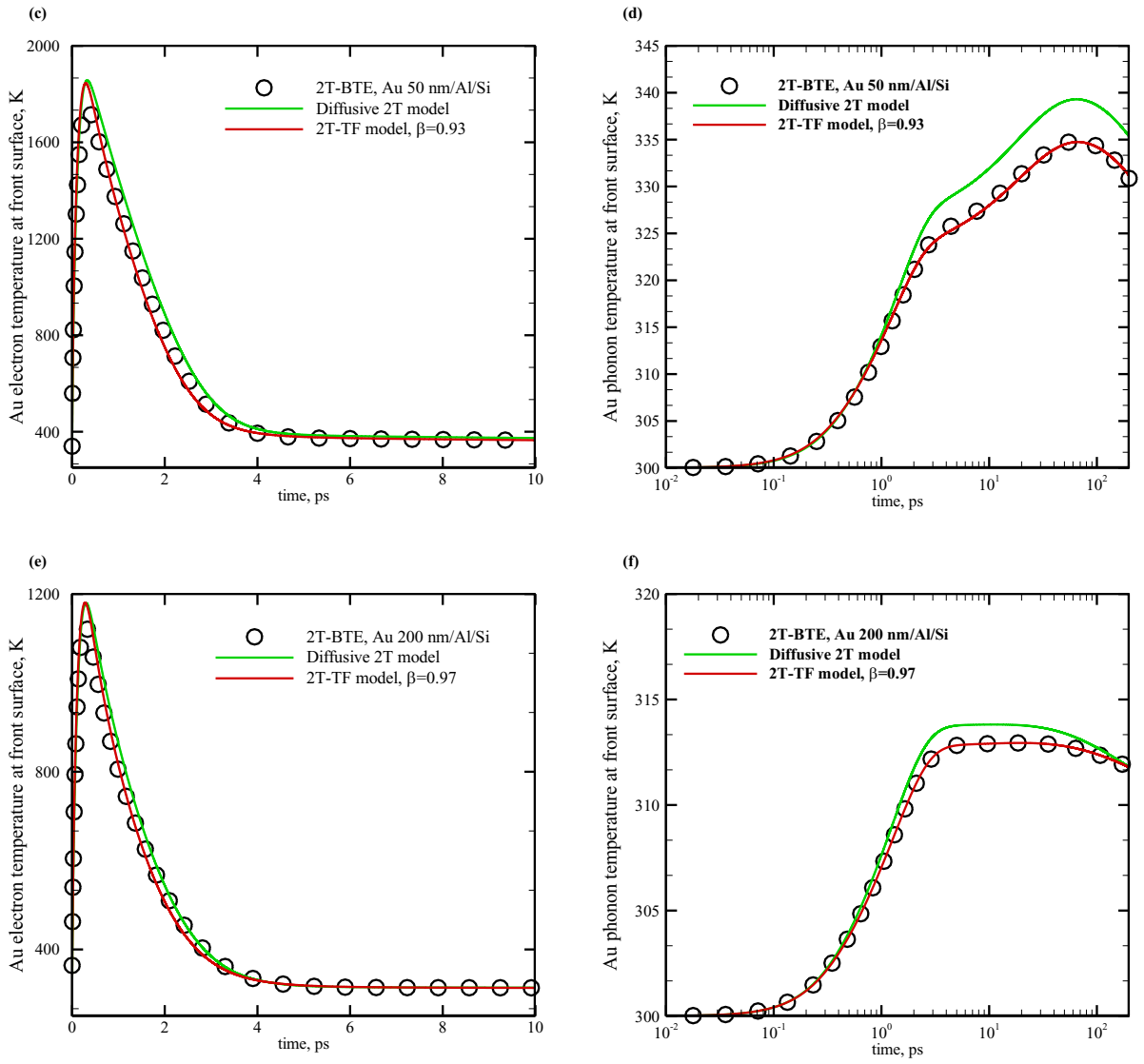

Fig. 10. Comparison between the diffusive 2T model, the 2T-TF model, and the 2T-BTE model in predicting the electron and phonon temperature evolution at the Au top layer of a Au film/Al interlayer/Si substrate heterostructure with different thicknesses of the top layer.

Notably, when the thickness of the top layer is only 10 nm, the diffusive 2T model suffers significant error in predicting electron temperatures. The failure of the diffusive 2T model occurs because the MFPs of both phonons and electrons are comparable to the thickness of the Au film, in which regime the Fourier-based model fails to capture non-diffusive behaviors. The significant non-diffusive thermal transport behavior is also reflected in the smaller value of $\beta = 0.81$ in the corresponding 2T-TF model. For the case of 20-nm-thick Au top layer, a value of $\beta = 0.9$ in the 2T-TF model provides accurate electron and lattice temperature evolutions of the Au layer, suggesting more diffusive thermal transport in thicker layers. Furthermore, for the cases of Au layer with thicknesses of 50 and 200 nm, β is equal to 0.93 and 0.97 respectively, indicating less significant ballistic effects. Correspondingly, as shown in Figs. (10e) and (10f), the diffusive 2T

model can predict the electron and phonon temperatures with good accuracy. Even so, there is still notable deviation of the phonon temperature (inside the top layer) predicted by the diffusive 2T model from that predicted by 2T-TF and 2T-BTE. Thus, we note that the parameter β in the 2T-TF model can serve as a direct measure of the level of non-diffusive thermal transport in the modeled system.

Fig. (11) illustrate the electron and phonon temperature distributions for thermal transport in a 10-nm Au/10-nm Al/100-nm Si thin film at various time instances. The phonon temperature of Au top layer increases because the Au layer lattice always heated up by the hot electrons of Au layer at earlier time instances, for example $t = 20$ ps. After that, a decreasing trend can be seen in lattice temperature of Au top layer, $t = 80$ ps, which is due to the thermal transport from Au layer to the Al interlayer. The lattice temperature distribution of Al interlayer first increases due to the EPI and also interfacial phonon transmission and then experiences a downward trend at the interface of interlayer/substrate because of losing thermal energy to the substrate lattice. The thermal transport from the interlayer lattice to the substrate can be observed in Figs. (11b, 11d and 11f). Also, the Si substrate lattice temperature increases at its interface with the interlayer due to the energy transmission from the hot interlayer lattice to the substrate. In the 2T-BTE approach, the heat carriers' velocities are explicitly considered, promising an accurate prediction of temperature distribution in the multilayered structures under ultrafast laser heating [10]. The terms $v_e.\nabla e_e$ and $v_p.\nabla e_p$ (where v and e represent the velocity and energy density of heat carriers, respectively) in the 2T-BTE approach can describe the thermal diffusion process and in particular the effects of carrier velocities on the diffusion process comprehensively. This is the main reason that the 2T-BTE approach can provide the most accurate prediction of thermal behaviors of multilayered thin films under ultrafast laser heating. However, such effects are only implicitly and approximately considered by the 2T-TF model presented in this work, and the deviation between the temperature distribution of different layers predicted by the 2T-TF model and 2T-BTE approach, especially for interlayer and substate, can be attributed to the effects of electron and phonon velocities on the thermal diffusion process. For example, for phonon temperature distribution, the comparison between Figs. (11d and 11f) reveals that this deviation is more significant for Al interlayer and Si substrate, but for Au top layer the results of 2T-TF model are reasonably matched with 2T-BTE's results. This is because the phonon velocities in Au top layer are less than those of Al interlayer and Si substrate [10], meaning that the effect of velocities on the thermal diffusion process is less significant, and thus the 2T-TF model can reasonably follow the 2T-BTE results. However, for Al and Si, electrons and phonons have higher velocities, which means that the thermal diffusion process can be more significantly affected by the heat carriers' velocities, and thus there can be a deviation between the temperature distribution predicted by the 2T-TF model and 2T-BTE method. This can be considered as a limitation for the time-fractional model proposed in this work. Still, we emphasize that the 2T-TF model is a significant improvement to the conventional diffusive 2T model, as this 2T-TF predicts thermal behaviors closer to those predicted by 2T-BTE.

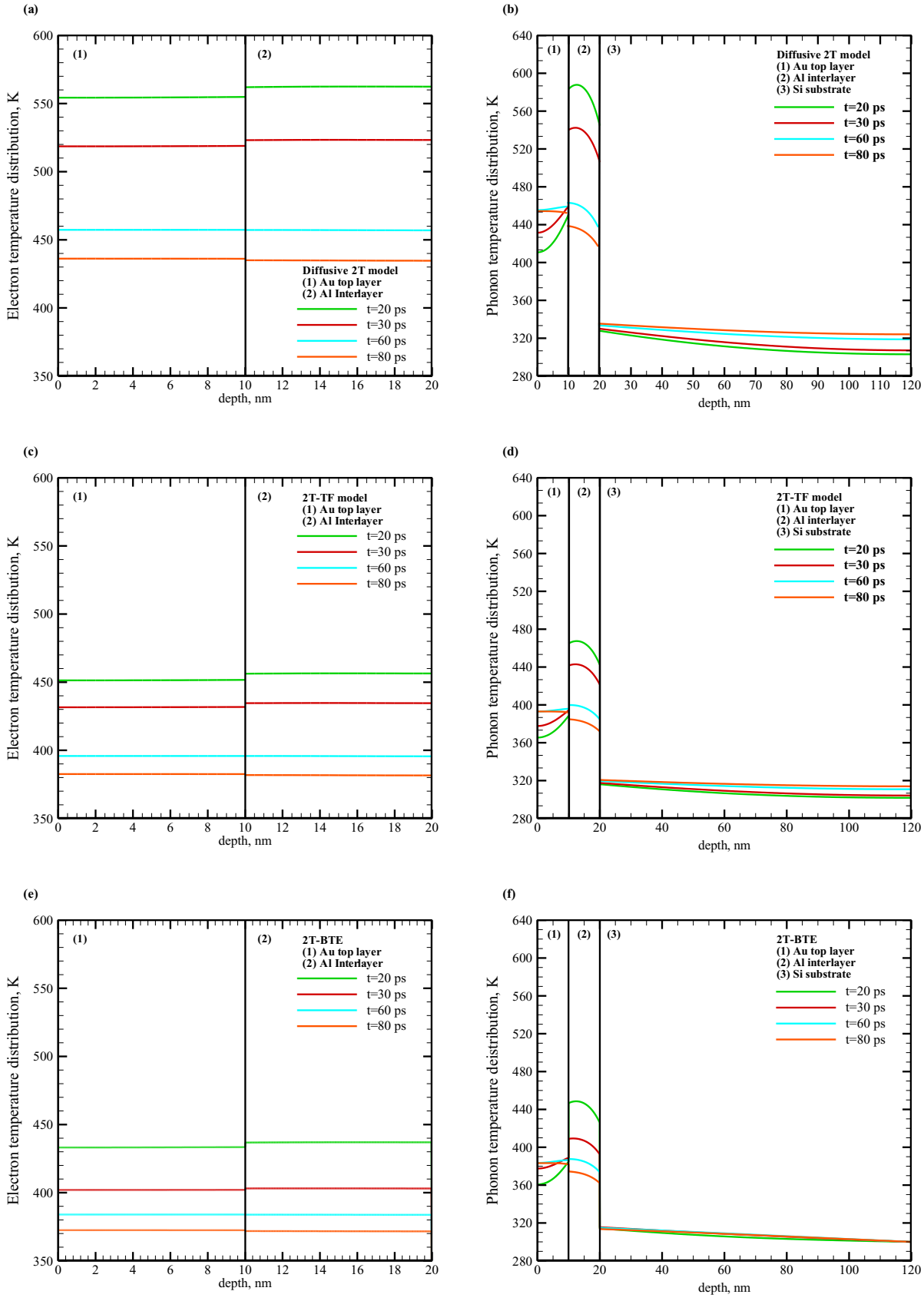
(a)
Electron temperature distribution, K
depth, nm
(1)
(2)
Diffusive 2T model
(1) Au top layer
(2) Al Interlayer
t=20 ps
t=30 ps
t=60 ps
t=80 ps
(b)
Phonon temperature distribution, K
depth, nm
(1)
(2)
(3)
Diffusive 2T model
(1) Au top layer
(2) Al interlayer
(3) Si substrate
t=20 ps
t=30 ps
t=60 ps
t=80 ps
(c)
Electron temperature distibution, K
depth, nm
(1)
(2)
2T-TF model
(1) Au top layer
(2) Al Interlayer
t=20 ps
t=30 ps
t=60 ps
t=80 ps
(d)
Phonon temperature distribution, K
depth, nm
(1)
(2)
(3)
2T-TF model
(1) Au top layer
(2) Al interlayer
(3) Si substrate
t=20 ps
t=30 ps
t=60 ps
t=80 ps
(e)
Electron temperature distribution, K
depth, nm
(1)
(2)
2T-BTE
(1) Au top layer
(2) Al Interlayer
t=20 ps
t=30 ps
t=60 ps
t=80 ps
(f)
Phonon temperature deistribution, K
depth, nm
(1)
(2)
(3)
2T-BTE
(1) Au top layer
(2) Al interlayer
(3) Si substrate
t=20 ps
t=30 ps
t=60 ps
t=80 ps

Fig. 11. Electron and phonon temperature distributions at different time instants predicted by diffusive 2T model, 2T-TF model with $\beta = 0.81$, and 2T-BTE.

Finally, we emphasize that the advantage of the 2T-TF model over 2T-BTE is the much lower computational cost and complexity of numerical implementation. This advantage is expected to be even more significant when we need to perform 2D or 3D simulations. As discussed in Wang et al.'s work [10], the coupling between electron and phonon BTEs requires a sophisticated design of computational mesh size or time step size. Specifically, the orders-of-magnitude difference in electron velocity and phonon velocity demands the use of similarly different mesh size or time step size for electron BTE and phonon BTE, which usually leads to a very dense mesh in the phonon BTE. In contrast, the numerical solution of 2T-TF much resembles that for the conventional heat diffusion equation, in which case the electron and phonon time fractional equations can be solved on the same mesh with the same time step size. Thus, the 2T-TF model can serve as a useful tool for modeling and interpret ultrafast, micro-/nano-scale thermal transport with less computational cost and less complexity in numerical implementation to replace the BTE approach, especially in many cases that do not need an extremely high accuracy. In addition, the fractional model can be used to reliably model the thermal behaviors of metal-nonmetal heterojunction systems. We have shown in this work that the 2T-TF model can describe a wide range of thermal behaviors, including the diffusive, quasi-ballistic and ballistic transport. However, this 2T-TF model only considers lumped phonon and electron modes, which cannot capture any nonequilibrium among phonon modes and among electron modes. In those scenarios, the phonon channel or electron channels must be further divided into more detailed sub-channels. For instance, we have demonstrated in our recent work [53] that the nonequilibrium between phonon modes can affect thermal transport in superlattice systems greatly.

Conclusion

To summarize, the Caputo-type time-fractional form of 2T model has been developed, which was referred to as 2T-TF model in our manuscript. This 2T-TF model can capture a wide range of thermal transport behaviors, including diffusive, quasi-ballistic, and ballistic transport, in micro-/nano-sized heterostructures under ultrafast laser irradiation. Interfacial electron and phonon transmissions can be readily implemented in the 2T-TF model, which were shown to considerably affect the heat dissipation of thin films irradiated by the femtosecond laser pulses. Cases studies on Au/Si heterostructures with and without a metallic interlayer were performed to evaluate the accuracy of the 2T-TF model, using the 2T-BTE model results as benchmarks. Our simulations demonstrated that the 2T-TF model can well match 2T-BTE results, significantly advantageous over the diffusive 2T model in modeling thermal transport in nanosized systems under ultrafast laser heating. Moreover, the computational cost and complexity of numerical implementation of the proposed 2T-TF model is superior to 2T-BTE. The non-Fourier 2T-TF model developed in this work will be useful for thermal modeling of nanoscale/microscale electronic and photonic devices as well as laser manufacturing processes, particularly those extreme manufacturing processes using ultrafast lasers to process micro-/nanomaterials.

Acknowledgment

The authors appreciate the financial support from National Science Foundation (CMMI-1826392 and CMMI-1825576). The authors would like to acknowledge the support of Research & Innovation and the Cyberinfrastructure Team in the Office of Information Technology at the University of Nevada, Reno for facilitation and access to the Pronghorn High-Performance Computing Cluster.

References

[1] J. Ghazanfarian, Z. Shomali, A. Abbassi, Macro- to nanoscale heat and mass transfer: The lagging behavior, International Journal of Thermophysics 36 (2015) 1416-1467.

[2] V.P. Carey, G. Chen, C. Grigoropoulos, M. Kaviany, A. Majumdar, A Review of Heat Transfer Physics, Nanoscale and Microscale Thermophysical Engineering 12 (1) (2008) 1-60.

[3] S. Lefèvre, S. Volz, P.O. Chapuis, Nanoscale heat transfer at contact between a hot tip and a substrate, International Journal of Heat and Mass Transfer 49 (1-2) (2006) 251-258.

[4] D.Y. Tzou, Macro- to microscale heat transfer: The lagging behavior, Second edition, Willey (2014).

[5] C. Kerse, H. Kalaycıoğlu, P. Elahi, B. Çetin, D.K. Kesim, Ö. Akçaalan, S. Yavaş, M.D. Aşık, B. Öktem, H. Hoogland, R. Holzwarth F.Ö. Ilday, Ablation-cooled material removal with ultrafast bursts of pulses, Nature 573 (2016) 84-88.

[6] R.R. Gattass, E. Mazur, Femtosecond laser micromachining in transparent materials, Nature Photonics 2 (2008) 219-225.

[7] T. Karkantonis, V. Nasrollahi, P. Penchev, S. Dimov, MHz burst mode processing as a tool for achieving removal rates scalability in ultrashort laser micro-machining, Applied Physics A 128 (2022) 711.

[8] A. Majumdar, P. Reddy, Role of electron–phonon coupling in thermal conductance of metal–nonmetal interfaces, Applied Physics Letter 84 (2004) 4768.

[9] Y. Wang, X. Ruan, A.K. Roy, Two-temperature nonequilibrium molecular dynamics simulation of thermal transport across metal-nonmetal interfaces, Physical Review B 85 (2012) 205311.

[10] Y. Wang, Z. Lu, A.K. Roy, X. Ruan, Effect of interlayer on interfacial thermal transport and hot electron cooling in metal-dielectric systems: An electron-phonon coupling perspective, Journal of Applied Physics 119 (2016) 065103.

[11] Z. Lu, Y. Wang, X. Ruan, Metal/dielectric thermal interfacial transport considering cross-interface electron-phonon coupling: Theory, two-temperature molecular dynamics, and thermal circuit, Physical Review B 93 (2016) 064302.

[12] T.Q. Qiu, C.L. Tien, Short-pulse laser heating on metals, International Journal of Heat and Mass Transfer 35 (3) (1992) 719-726.

[13] T.Q. Qiu, C.L. Tien, Heat transfer mechanisms during short-pulse laser heating of metals, Journal of Heat Transfer 115 (1993) 835-841.

[14] T.Q. Qiu, C.L. Tien, Femtosecond laser heating of multi-layer metals-I. Analysis, International Journal of Heat and Mass Transfer 37 (17) (1994) 2789-2797.

[15] T.Q. Qiu, T. Juhasz, C. Suarez, W.E. Bron, C.L. Tien, Femtosecond laser heating of multi-layer metals-II. Experiments, International Journal of Heat and Mass Transfer 37 (17) (1994) 2799-2808.
[16] Y. Gan, J.K. Chen, Thermomechanical wave propagation in gold films induced by ultrashort laser pulses, Mechanics of Materials 42 (2010) 491-501.
[17] B.C. Chen, Y.C. Lee, C.Y. Ho, M.Y. Wen, Y.H. Tsai, Analysis of removal region in nanoscale metal film processed by ultrafast-pulse laser, Computational Materials Science 117 (2016) 590-595.
[18] I. Milov, V. Lipp, N. Medvedev, I.A. Makhotkin, E. Louis, F. Bijkerk, Modeling of XUV-induced damage in Ru films: the role of model parameters, Journal of the Optical Society of America B 35 (10) (2018).
[19] A. Nicarel, M, Oane, I.N. Mihailescu, C. Ristoscu, Fourier two-temperature model to describe ultrafast laser pulses interaction with metals: A novel mathematical technique, Physics Letter A 15 (2021) 127115.
[20] D.G. Cahill, Nanoscale thermal transport, Journal of Applied Physics 93 (793) (2003).
[21] D.G. Cahill, P.V. Braun, G. Chen, D.R. Clarke, S. Fan, K.E. Goodson, P. Keblinski, W.P. King, Gerald D. Mahan, A. Majumdar, H.J. Maris, S.R. Phillpot, E. Pop, Li Shi, Nanoscale thermal transport II, Applied Physics Reviews 1 (2014) 011305.
[22] J.K. Chen, D.Y. Tzou, J.E. Beraun, A semiclassical two-temperature model for ultrafast laser heating, International Journal of Heat and Mass Transfer 49 (2006) 307-316.
[23] K.V. Poletkin, G.G. Gurzadyan, J. Shang, V. Kulish, Ultrafast heat transfer on nanoscale in thin gold films, Applied Physics B 107 (2012) 137-143.
[24] A.E. Abouelregal, Two-temperature thermoelastic model without energy dissipation including higher order time-derivatives and two phase-lags, Materials Research Express 6 (2019) 116535.
[25] G. Mittal, V.S. Kulkarni, Two temperature fractional order thermoelasticity theory in a spherical domain, Journal of Thermal Stresses 42 (9) (2019) 1136–1152.
[26] I. Abbas, T. Saeed, M. Alhothuali, Hyperbolic two-temperature photo-thermal interaction in a semiconductor medium with a cylindrical cavity, Silicon 13 (2021) 1871–1878.
[27] S. Shen, W. Dai, J. Cheng, Fractional parabolic two-step model and its accurate numerical scheme for nanoscale heat conduction, Journal of Computational and Applied Mathematics 375 (2020) 112812.
[28] C.Y. Ho, M.Y. Wen, B.C. Chen, Y.H. Tsai, Non-Fourier two-temperature heat conduction model used to analyze ultrashort-pulse laser processing of nanoscale metal film, Journal of Nanoscience and Nanotechnology 14 (2014) 5581–5586.
[29] M.L. Huberman, Electronic Kapitza conductance at a diamond-Pb interface, Physical Review B 4 (1994).
[30] A.V. Sergeev, Electronic Kapitza conductance due to inelastic electron-boundary scattering, Physical Review B 58 (1998).
[31] R.M. Costescu, M.A. Wall, D.G. Cahill, Thermal conductance of epitaxial interfaces, Physical Review B 67 (2003) 054302.
[32] A. Giri, B.M. Foley, P.E. Hopkins, Influence of hot electron scattering and electron-phonon interactions on thermal boundary conductance at metal/nonmetal interfaces, Journal of Heat Transfer 136 (2014).

[33] Y.R. Koh, J. Shi, B. Wang, R. Hu, H. Ahmad, S. Kerdsongpanya, E. Milosevic, W.A. Doolittle, D. Gall, Z. Tian, S. Graham, P.E. Hopkins, Thermal boundary conductance across epitaxial metal/sapphire interfaces, Physical Review B 102 (2020) 205304.
[34] F. Krahl, A. Giri, M.S.B. Hoque, L. Sederholm, P.E. Hopkins, M. Karppinen, Experimental Control and Statistical Analysis of Thermal Conductivity in ZnO–Benzene Multilayer Thin Films, The Journal of Physical Chemistry C 124 (45) (2020) 24731-24739.
[35] A. Giri, M.V. Tokina, O.V. Prezhdo, P.E. Hopkins, Electron–phonon coupling and related transport properties of metals and intermetallic alloys from first principles, Materials Today Physics 12 (2020) 100175.
[36] B.C. Gundrum, D.G. Cahill, R.S. Averback, Thermal conductance of metal-metal interfaces, Physical Review B 72 (2005) 245426.
[37] P.E. Hopkins, P.M. Norris, Thermal boundary conductance response to a change in Cr/Si interfacial properties, Applied Physics Letter 89 (2006) 131909.
[38] B.F. Donovan, C.J. Szwejkowski, J.C. Duda, R. Cheaito, J.T. Gaskins, C.Y.P. Yang, C. Constantin, R.E. Jones, P.E. Hopkins, Thermal boundary conductance across metal-gallium nitride interfaces from 80 to 450 K, Applied Physics Letter 105 (2014) 203502.
[39] L. Guo, S.L. Hodson, T.S. Fisher, X. Xu, Heat transfer across metal-dielectric interfaces during ultrafast-laser heating, Journal of Heat Transfer 134 (2012).
[40] M. Mozafarifard, D. Toghraie, Time-fractional subdiffusion model for thin metal films under femtosecond laser pulses based on Caputo fractional derivative to examine anomalous diffusion process, International Journal of Heat and Mass Transfer 153 (2020) 119592.
[41] M. Mozafarifard, S.M. Mortazavinejad, D. Toghraie, Numerical simulation of fractional non-Fourier heat transfer in thin metal films under short-pulse laser, International Communications in Heat and Mass Transfer 115 (2020) 104607.
[42] I. Podlubny, Fractional Differential Equations, Academic Press, New York, 1999, pp. 41-81.
[43] Z. Lin, L.V. Zhigilei, Electron-phonon coupling and electron heat capacity of metals under conditions of strong electron-phonon nonequilibrium, Physical Review B 77 (2008) 075133.
[44] D.Y. Tzou, A unified field approach for heat conduction from macro- to micro-scales, Journal of Heat Transfer 117 (1995) 8-16.
[45] P. Jiang, X Qian, R. Yang, Time-domain thermoreflectance (TDTR) for thermal property characterization of bulk and thin film materials, Journal of Applied Physics 124 (2018) 161103.
[46] E. T. Swartz, R. O. Pohl, Thermal boundary resistance, Reviews of Modern Physics 61 (1989) 605.
[47] W. Zhang, T.S. Fisher, N. Mingo, The Atomistic Green's Function Method: An Efficient Simulation Approach for Nanoscale Phonon Transport, Numerical Heat Transfer Part B Fundamentals 51 (4) (2007) 333-349.
[48] Y. Wang, Z. Lu, X. Ruan, First-principles calculations of lattice thermal conductivities of metals considering phonon-phonon and phonon-electron scattering, Journal of Applied Physics 119 (2016) 225109.

[49] T. Ma, P. Chakraborty, X. Guo, L. Cao, Y. Wang, First-principles Modeling of Thermal Transport in Materials: Achievements, Opportunities, and Challenges, International Journal of Thermophysics 41 (2020) 4.
[50] D.W. Tang, N. Araki, Wavy, wavelike, diffusive thermal responses of finite rigid slabs to high-speed heating of laser-pulses, International Journal of Heat and Mass Transfer 42 (1999) 855-860.
[51] I.H. Chowdhury, X. Xu, Heat transfer in femtosecond laser processing of metal, Numerical Heat Transfer Part A: Applications 44 (3) (2003) 219-232.
[52] J. Hohlfeld S.S. Wellershoff, J. Güdde, U. Conrad, V. Jähnke, E. Matthias, Electron and lattice dynamics following optical excitation of metals, Chemical Physics 251 (1-3) (2000) 237-258.
[53] T. Ma, Y. Wang, Ex-situ modification of lattice thermal transport through coherent and incoherent heat baths, Materials Today Physics 29 (2022) 100884.